Near-surface modification of defective KTaO3 by ionizing ion irradiation

G Velişa, E Zarkadoula, D Iancu, M Mihai, C Grygiel, I Monnet, B Kombaiah, Y Zhang, W Weber

Near-surface modification of defective $KTaO_3$ by ionizing ion irradiation

G. Velişa[a,b,e*], E. Zarkadoula[b], D. Iancu[a,f], M.D. Mihai[a], C. Grygiel[d], I. Monnet[d], B. Kombaiah[b], Y. Zhang[b,c], and W.J. Weber[c,b**]

[a]Horia Hulubei National Institute for Physics and Nuclear Engineering, Măgurele, IF 077125, Romania
[b]Materials Science and Technology Division, Oak Ridge National Laboratory, Oak Ridge, TN 37831, USA
[c]Department of Materials Science & Engineering, University of Tennessee, Knoxville, TN 37996, USA
[d]Centre de Recherche sur les Ions, les Matériaux et la Photonique, CEA, CNRS, ENSICAEN, UNICAEN, Normandie Université, 14070 Caen, France
[e]Extreme Light Infrastructure–Nuclear Physics (ELI–NP), Măgurele, IF 077125, Romania
[f]University of Bucharest, Faculty of Physics, Măgurele, IF 077125, Romania

Abstract

The synergistic effect of nuclear (S_n) and electronic (S_e) energy loss observed in some ABO_3 has attracted considerable attention due to the real possibility to modify various near-surface properties, such as the electronic and optical properties, by patterning ion tracks in the defective near-surface regions. In this study, we show that low-energy ion-induced disordering in conjunction with ionizing ion irradiation (18 MeV Si, 21 MeV Ni and 91.6 MeV Xe) is a promising approach for tailoring ion tracks in the near-surface of defective $KTaO_3$. Experimental characterization and computer simulations reveal that the size of these latent ion tracks increases with S_e and level of pre-existing damage. These results further reveal that the threshold S_e value (S_e^{th}) for track creation increases with decreasing pre-damage level. The values of S_e^{th} increase from 5.02 keV/nm for a pre-existing fractional disorder of 0.53 to 10.81 keV/nm for pristine $KTaO_3$. Above these thresholds, amorphous latent tracks are produced due local melting and rapid quenching. Below a disorder fraction of 0.08 and $S_e \leq 6.68$ keV/nm, the synergistic effect is not active, and damage accumulation is suppressed due to a competing ionization-induced damage annealing process. These results indicate that, depending on S_e and the amount of pre-existing damage, highly ionizing ions can either enhance or suppress damage accumulation in $KTaO_3$, thus providing a pathway to tailoring defects states. Comprehending the conflicting roles of highly ionizing ions in defective ABO_3 oxides is vital for understanding and predictive modeling of ion-solid interactions in complex oxides, as well as for achieving control over ion track size in the near-surface of defective $KTaO_3$.

* Corresponding author. Horia Hulubei National Institute for Physics and Nuclear Engineering, Măgurele, IF 077125, Romania
E-mail addresses: gihan.velisa@nipne.ro (Gihan Velişa), Tel: +4 0723-933-922

** Corresponding author. Materials Science and Engineering, University of Tennessee, Knoxville, TN 37006, USA.
E-mail addresses: wjweber@utk.edu (William J. Weber), Tel: +1 865-974-0415

Keywords: Perovskites, Ion irradiation, RBS/C, MD simulation, Ion track

1. Introduction

Near-surface modification by ion beams is still an open research topic in material science because it allows tailoring material properties by accurately controlling microstructural modifications at the atomic level [1–8]. Experimental studies [4,9,10] have revealed that ion irradiation is a promising technique to manipulate various near-surface properties of complex oxides, such as ABO_3 perovskites. The most studied near-surface property changes in perovskite materials include modified electronic [11–16] and optical [3,10,17–19] properties. Research has shown that irradiation of $KTaO_3$ with inert noble gases, having energies within the keV to MeV range, enables new functionalities of $KTaO_3$. For example, low-energy Ar irradiation has been successfully applied in the transformation of $KTaO_3$ from an insulator to a conducting material by creating oxygen vacancies [12]. On the other hand, impurities and defect scattering, which are intrinsically associated with both ion implantation [20–22] and ion irradiation [11,12] processes, can limit the mobility of electrons, particularly at low temperatures. Consequently, ion-beam processing can have contrasting effects on near-surface properties of materials. Thus, understanding and predicting the relationships between ion-irradiation conditions and damage evolution in $KTaO_3$ are critical for a diverse range of applications.

Since $KTaO_3$ and related oxide perovskites have been put forward as candidate materials to immobilize radioactive waste, several previous investigations [23–25] have mimicked the self-radiation effects of alpha decay, which produces alpha particles and recoil nuclei, by using low-energy ions that primarily undergo collisional energy loss with target nuclei (S_n). These studies have reported that collisional-damage accumulation leads to complete amorphization in $KTaO_3$, if the irradiation is performed below the critical amorphization temperature, T_c. Research has shown that T_c in $KTaO_3$ ranges from 640 to 880 K and decreases with decreasing ion mass [23,24].

Researchers have shown that the formation of buried amorphous layers for waveguide barriers in $KTaO_3$ via noble gas ion irradiation (e.g., He [26]) requires relatively high fluences that can lead to gas bubbles forming [4]. In this respect, heavier ions (e.g., Ar [4]) are more effective for generation of buried amorphous layers, because the ion fluences needed for amorphization are lower than for lighter ions. However, obtaining equivalent buried layer thicknesses, (typically a few micrometers), as in the case of helium ion irradiations, requires much higher ion energies [4]. Since electronic energy loss (S_e) constitutes the main deceleration process for high energy particles, the understanding of electronic excitations and ionization processes driven by S_e is important for the production of electro-optical devices based on nanoscale phase transformations and defects induced in the crystal structure by highly-ionizing ions.

Although irradiation with highly-ionizing ions provides a potential approach to the fabrication of waveguides in perovskites (e.g., $KTaO_3$), the response of $KTaO_3$ to such high-energy ions has not been studied in as much detail as low-energy ion-induced disordering and amorphization in $KTaO_3$ [23–25,27]. In fact, only one study [18] has focused on irradiation of $KTaO_3$ with swift heavy ions (SHIs), and they reported that irradiation of $KTaO_3$ with SHIs (358 MeV Ni, with S_e ~13.8 keV/nm) results in discontinuous latent ion track formation in pristine $KTaO_3$. An ion track in materials is a cylindrical column of either defective crystalline or amorphous material along the ion path, which forms upon rapid quenching of a molten or high-temperature state produced by the dissipation of high electronic energy density via electron-phonon coupling to the atomic subsystem [4]. It has been demonstrated that the dimensions and structure of the ion tracks are dependent on S_e and material composition [4]. Moreover, there is generally a composition-dependent threshold in S_e (S_e^{th}) above which tracks are formed. Research has shown that the S_e^{th} value may be less than 1 keV/nm for polymers; whereas for metals, it can greater than several tens of keV/nm [28]. It has also been

demonstrated that there is generally a substantial dependence of S_e^{th} values for track formation on compositional changes within the same crystal structure. For example, the experimentally-measured S_e^{th} for formation of discontinuous tracks in pristine $SrTiO_3$ is about 10 keV/nm [29]; whereas for pristine $KTaO_3$, it is determined to be 13.8 keV/nm [18].

A previous experimental study on the sensitivity of pre-damaged $SrTiO_3$ to highly-ionizing ions has indicated that pre-existing defects have a synergistic effect on the dissipation of electronic energy that enables the creation of amorphous tracks over the region of pre-existing damage [30]. They reported that the S_e^{th} value for amorphous track creation in pre-damaged $SrTiO_3$ is about 6.7 keV/nm. It is evident that the synergistic interaction between the highly-ionizing ions and pre-existing defects dramatically reduces the S_e^{th} value (i.e., from 10 keV/nm to 6.7 keV/nm) for creation of such tracks. This same experimental study has also revealed that the diameter of the tracks increases with the amount of pre-existing damage and S_e of the incident ions. Molecular dynamics (MD) simulations have confirmed this synergistic stimulation of amorphous track creation in both pre-damaged $SrTiO_3$ [31] and $KTaO_3$ [32] for conditions corresponding to 21 MeV Ni ion irradiation (S_e ~ 9.9 and 10.16 keV/nm in $SrTiO_3$ and $KTaO_3$, respectively). This synergistic effect in $KTaO_3$ was later experimentally validated using 21 MeV Ni ions in a study on the irradiation response of pre-damaged $KTaO_3$ [33]. This same experimental study also revealed that no measurable damage was produced in pristine $KTaO_3$ (see inset of Fig. S1a), which suggests that the S_e^{th} value for track creation in pristine $KTaO_3$ is greater than 10.16 keV/nm. Furthermore, this study reported that the effective track diameter increases linearly with increasing S_e for low disorder levels, while track size tends to saturate at high values of S_e and high disorder levels [33]. The existence of this dependence was further corroborated by MD simulations [34]. More recently, Han et al. [18] have indicated thresholds of about 12.0 and 13.8 keV/nm, respectively, for the creation of spherical defects and discontinuous tracks in pristine $KTaO_3$ with 358 MeV Ni ions, which are in the

high velocity regime (i.e., ion energy above the peak in S_e). However, none of the existing experimental and theoretical studies have determined S_e^{th} for this synergistic effect nor the dependence of S_e^{th} on pre-damage levels in $KTaO_3$.

Although the synergistic coupling of S_e dissipation with pre-existing defects may dramatically enhance damage accumulation in some ABO_3 oxides, as revealed by the measured rapid amorphization driven by track formation, this defect-stimulated track formation may also have beneficial applications, such as the change in refractive index relative to the pristine bulk crystal [3,35–37] that enables fabrication of waveguides and other optical functionalities in the near-surface of defective $KTaO_3$ [17,18,38]. Since the electronic conductivity of ion tracks (conducting material) may be enhanced relative to the bulk insulating material, these conductive ion tracks may also be employed as durable field emission cathodes [39]. Further development of these applications requires an improved understanding of the spatial distribution, radial structure and radial stress of the ion tracks [4]. A precise determination of how ion track creation depends on S_e and initial damage-state may offer new possibilities to better control the properties of ion tracks and their interfaces with the surrounding matrix [40]. Therefore, the determination of the S_e^{th} value for track formation and how it depends on initial pre-damage state can facilitate the selective design of ion tracks in the near-surface of $KTaO_3$ by ion beams, which may provide new flexible approaches to tailor the properties or functionality of perovskite materials for electro-optical applications.

In this study, the synergistic coupling of pre-existing defects with S_e dissipation is explored in pre-damaged $KTaO_3$ irradiated with 18 MeV Si ions and 91.6 MeV Xe ions at 300 K, and the results are compared with those previously obtained using 21 MeV Ni ions [33]. In this work, all ions are in the low velocity regime (i.e., below the peak in S_e) and the ion energies yield S_e values below and above those reported for ionization-induced track creation in pre-damaged $KTaO_3$ irradiated at a flux of 6×10^{10} ions/cm^2·s with 21 MeV Ni ions [33]. As

aforementioned, accurate information on the S_e^{th} value is still missing and thus, a combined experimental and computational evaluation is employed to determine the S_e^{th} values for this synergistic effect and the dependence of S_e^{th} on the pre-damage level.

2. Experimental Procedures and Modelling

2.1. Irradiation and characterization

One set of three epi-polished, ⟨100⟩-oriented, single crystal $KTaO_3$ wafers were pre-damaged at 300 K via irradiation with 2.0 MeV Au^{2+} ions to ion fluences of 6.4×10^{12}, 1.1×10^{13}, and 1.6×10^{13} ions/cm^2, with an average particle flux of 1.6×10^{10} ions/cm^2·s, using the 3 MV Tandetron Cockcroft-Walton accelerator at IFIN-HH [41]. Irradiations with Au ions were carried out along a random-equivalent direction by tilting the sample 7° off the ⟨100⟩ orientation. A 2 MeV He beam was employed to perform ex-situ Rutherford backscattering spectrometry in a channeling configuration (RBS/C) along the ⟨100⟩ direction and along a random (off-channel) direction on the pristine $KTaO_3$ and on each irradiated area to evaluate the corresponding change in level of fractional disorder. The RBS/C measurements were performed with the silicon detector positioned at 165° from the direction of the incident beam. The disorder depth profile associated with each RBS/C spectrum was determined based on an iterative method that was originally applied to $SrTiO_3$ [42] and later used to quantify the irradiation-induced disorder in $KTaO_3$ [25]. In this analysis, a fractional disorder level of 0.0 refers to the unirradiated or pristine state, and a fractional disorder level of 1.0 corresponds to a random or completely amorphous structure. The initial maximum disorder fractions, f_0, created in 2 MeV Au-irradiated $KTaO_3$ to fluences of 6.4×10^{12}, 1.1×10^{13}, and 1.6×10^{13} ions/cm^2 were 0.08, 0.30 and 0.53 on the Ta sublattice, respectively. In a previous study [25], we have shown that for $KTaO_3$ irradiated with low-energy noble gases at 300 K the damage accumulation exhibits a slow damage accumulation rate at low fluences (often referred to as step 1) and followed by a sharp rise of the accumulated damage (often referred to as step 2)

with ion fluence before amorphous state is achieved. In other word, these damage accumulation curves exhibit sigmoidal behavior that was well described by a comprehensive damage accumulation model. The model curve fits to the experimental data, have demonstrated that point defects (and small point defect clusters) and amorphous nuclei are produced in step 1 (relative disorder level ≤ 0.08) and 2, respectively. One should note that the formation of larger defect clusters is disregarded in this model fits because their formation is inhibited due to the nucleation of amorphous seeds at very early stages of damage accumulation. Since the sample with $f_0 = 0.08$ corresponds to the end of step 1 just before the sharp increase of the accumulated damage, only point defects (and small point defect clusters) are expected to form in the sample irradiated to 1.6×10^{13} ions/cm^2. The sample with $f_0 = 0.3$ and 0.53 corresponds to the beginning and middle of step 2, respectively. Thus, a larger amorphous fraction is to be expected in the sample irradiated to 1.6×10^{13} ions/cm^2 than in the sample irradiated to 1.1×10^{13} ions/cm^2. Afterwards, these pre-damaged $KTaO_3$ samples were subjected to irradiation at 300 K with 18 MeV Si^{6+} ions to fluences ranging from 1.0×10^{12} to 1.0×10^{13} ions/cm^2. The average ion flux was 2.1×10^9 ions/cm^2·s to prevent macroscopic heating and maintain the 300 K irradiation temperature. Pristine $KTaO_3$ was also irradiated with 18 MeV Si ions under identical conditions for reference. The evolution of disorder with increasing ion fluence in these irradiated samples was evaluated by RBS/C utilizing a 2.0 MeV He beam, as described above.

Another set of two ⟨100⟩-oriented $KTaO_3$ single-crystal wafers were each pre-damaged via irradiation at 300 K with 2.0 MeV Au^{2+} ions to an ion fluence of 6.4×10^{12} ions/cm^2 utilizing the capabilities of 3 MV tandem accelerator facility in the Ion Beam Materials Laboratory (IBML) on the campus of the University of Tennessee [43]. The average ion flux to pre-damage the samples was 2.7×10^{11} ions/cm^2·s, which was estimated to increase the sample temperature by less than 15 K. To minimize the effects of incident ion channeling

during the irradiations, all irradiations were implemented along a random direction by tilting the crystal 7° off the surface normal. In-situ RBS/C, which were performed with 2.0 MeV He ions and with the silicon detector positioned at 155° from the incident beam direction, determined the damage profile and a peak disorder fraction of 0.08 on the Ta sublattice in the pre-damaged $KTaO_3$. A higher level of disorder was also produced at 300 K in another two $KTaO_3$ wafers by 2.0 MeV Au ion irradiation to a fluence of 1.2×10^{13} ions/cm^2, which resulted in a peak disorder fraction of about 0.33 for these pre-damaged samples. The pristine and four pre-damaged samples were then irradiated at the GANIL facility (Caen, France) on the IRRSUD beamline using 91.6 MeV ^{129}Xe ions to ion fluences of 1.0×10^{11} and 1.0×10^{12} ions/cm^2. As in the case of the 18 MeV Si ion irradiations, the ion flux was 2×10^9 ions/cm$^2\cdot$s to prevent sample heating. Disorder modifications in these SHI irradiated samples at each fluence were determined utilizing RBS/C with a 2.0 MeV He beam, as described above.

The mean projected range of 2 MeV Au ions in $KTaO_3$ has been determined based on SRIM simulations [44], which yielded a projected ion range, R_P, of ~260 nm and range straggling, ΔR_P, of ~82 nm. Based on SRIM calculations, the ion fluences of 6.4×10^{12} to 1.6×10^{13} ions/cm^2 result in a peak concentration of implanted Au ions of ~0.0006 to ~0.001 at. %, respectively. Consequently, under these conditions, the damage evolution processes in $KTaO_3$ are not expected to be significantly affected by changes in chemistry or local strain associated with the implanted Au ions. In the case of the higher energy ions, the ion ranges are substantially much larger (i.e., 4.5 and 7.85 μm in the case of 18 MeV Si and 91.6 MeV Xe ions, respectively). Therefore, the high energy ions come to rest substantially past the pre-damaged layer and do not add to measurable change in pre-damage disorder. The corresponding depth profile of damage dose, in displacements per atom (dpa), in $KTaO_3$ for 2 MeV Au irradiation has been ascertained by summing the K, Ta, and O vacancies and atomic replacements at each depth, which have been calculated using full-cascade SRIM simulations,

Table 1: SRIM predicted electronic energy loss (S_e), nuclear energy loss (S_n), and ratio S_e/S_n at a depth of 170 nm in $KTaO_3$ for each high energy ion used. The specific energy (E) is also included.

Ion/energy	S_e (keV/nm)	S_n (keV/nm)	S_e/S_n	E (MeV/u)
18 MeV ^{28}Si	6.16	0.018	342	0.64
21 MeV ^{58}Ni	10.16	0.121	84.0	0.36
91.6 MeV ^{129}Xe	23.18	0.220	105	0.71

as recently recommended [45]. In all SRIM calculations, the theoretical density for $KTaO_3$ (7.015 g/cm^3) was used, and a 25 eV displacement energy was assumed for all elements [23,24]. Additionally, the depth dependence of the projected energy losses, S_n and S_e, as well as the ratio S_e/S_n, were predicted using the SRIM code, and the values at the depth of the pre-damage peak are summarized in Table 1.

Both a pristine sample and a pre-damaged sample of $KTaO_3$ irradiated with 91.6 MeV Xe ions were also analyzed by transmission electron microscopy (TEM). A focused ion beam approach, followed by ion milling with low-energy Ar, was used for preparing the cross-sectional samples for TEM. The TEM results are provided in the Supplementary material.

2.2. Computer simulations of track evolution

Molecular dynamics simulations have been integrated with a model for the inelastic thermal spike [46] in order to evaluate the dissipation of S_e and evolution of ion tracks from irradiation with 18 MeV Si, 21 MeV Ni and 91.6 MeV Xe ions in pre-damaged $KTaO_3$. The model for the evolution of the inelastic thermal spike has its foundation in the two-temperature description of heat dissipation in the electronic and atomic subsystems, which describes the transfer of S_e to the atomic subsystem via electron-phonon coupling. As reported previously for $KTaO_3$ [32,34], the electronic energy dissipation profile transferred to the atomic structure for a given ion and energy is established by the inelastic thermal spike model. This calculated energy dissipation profile for each ion is incorporated as input to the

MD simulations to determine the response to each thermal spike event. For the thermal spike calculations in pre-damaged $KTaO_3$, we used lattice and electronic thermal conductivity reduced by a factor of ten compared to the values for pristine $KTaO_3$, as discussed previously [20]. The mean free electron path used for $KTaO_3$ with 11% pre-existing Frenkel pairs (FPs) is 2.2 nm and for $KTaO_3$ with 30% pre-existing FPs is 1.9 nm [20].

The DL_POLY code [47] was used for the MD simulations, with empirical potentials [48] smoothly merged to the ZBL scattering (repulsive) potentials [44] for close interatomic distances. The systems have a size of 26.5 nm × 26.5 nm × 60 nm and periodic boundaries. The initial disorder levels of 11 and 30% FPs were generated by randomly introducing FPs into the simulation cell, which is intended to qualitatively reproduce the presence of an initial fractional disorder peak, f_0, of ~0.11 and 0.30, respectively (see RBS/C results). The simulation cells with FPs were equilibrated under a constant temperature and pressure ensemble before injecting the thermal spike in the z direction of the simulation cell. The thermal-spike simulations were performed in the microcanonical ensemble. Energy scaling at the boundaries of the simulation cell along the x and y dimensions was applied using a Langevin thermostat with a width of 10 Å. A simple geometric criterion based on small sphere, with a cut-off radius of 0.75 Å, was used to distinguish defects [49] in the simulation cell.

3. Results

3.1 RBS/C results

The distributions of relative disorder with depth for the Au-irradiated $KTaO_3$, with and without subsequent irradiation with 18 MeV Si^{6+} ions, are shown in Figs. 1(a-c). These damage depth distributions were derived, using an iterative procedure [42], from the RBS/C spectra provided in Figs. S1(a-c) (supplementary material). Only best-fit curves to the actual data are provided for visual lucidity. In Fig. 1(b), the depth profile of local damage dose (dpa)

derived from full-cascade SRIM simulations for $KTaO_3$ irradiated with 2 MeV Au ions to 1.1×10^{13} ions/cm^2 is included for reference, and the peak in damage dose occurs at depth of about 170 nm. For the low initial disorder level of ~0.08 (Fig. 1a), subsequent 18 MeV Si ion irradiation to a relatively low fluence of 1.0×10^{12} ions/cm^2 causes a small decrease in the amount of disorder. Upon further irradiation to higher fluences, 1.0×10^{12} ions/cm^2 to 1.5×10^{12} ions/cm^2, the measured disorder slightly increases, but is still lower than the initial damage level of 0.08. Surprisingly, the measured disorder again starts to decrease slightly with increasing Si fluence from 1.5×10^{12} to 8.0×10^{12} ions/cm^2. On the other hand, for the higher initial levels of pre-existing disorder, f_0, in $KTaO_3$ (i.e., about 0.30 (Fig. 1b) and 0.53 (Fig. 1c)), subsequent irradiations with 18 MeV Si^{6+} ions dramatically enhance damage accumulation, as evidenced by the increase of fractional disorder over the entire damage profile with increasing Si fluence. This accelerated damage accumulation clearly indicates a synergistic coupling between energy dissipation by highly ionizing ions and pre-existing defects, which triggers ion track formation within the pre-damaged region [30,33]. One can note that the Ta disorder peak in the pre-damaged samples shifts slightly to deeper depths with increasing Au ion fluence or level of disorder. This is generally due to some relaxation of the irradiation-induced normal tensile strain and formation of defect clusters at the damage peak [50–53] in conjunction with the potential chemical effects of the implanted ion species [54]. Since the SRIM calculations indicate that the peak Au concentration does not exceed 0.001 at.%, the chemical effects of the implanted ions may be ruled out [55]. It is, however, important to also note that the peaks in increased disorder due to the 18 MeV Si ions are nearly at all the same depths (as predicted by the SRIM damage peak), independent of the Au ion fluence. This clearly suggests that the actual irradiation-induced pre-damage profiles are responsible for the synergistic effects. The oscillating changes in the relative disorder level with Si fluence at low initial disorder level, as shown in Fig. 1(a), indicates that for the sample

with the lowest initial damage level (~0.08), the synergistic effect is not active, and may in fact be competing with a damage annealing process, as observed in $SrTiO_3$ [56]. In other words, a threshold disorder level above 0.08, but below 0.30, is required to stimulate track formation in pre-damaged $KTaO_3$ with 18 MeV Si ions.

While there is no evidence for damage production in pristine $KTaO_3$ irradiated with 18 MeV Si ions (see inset of Fig. S1a), there is obvious evidence for disorder production in the pristine $KTaO_3$ following irradiation with 91.6 MeV Xe ions (see Fig. S2(a) in the supplementary material). Similar disorder production was also previously observed in pristine $SrTiO_3$ irradiated with SHIs (629 MeV Xe and 946 MeV Au) [40]; whereas in pristine $SrTiO_3$ irradiated with lower energy and lighter mass ions (i.e., lower S_e), no measurable damage was produced [30]. Following the approach of Xue et al. [40] for analysis of the RBS/C spectra from pristine and pre-damaged $SrTiO_3$ irradiated with SHIs, the net growth in RBS yield, $\chi(n)_{net}$, for channel number, n, has been determined for the pre-damaged $KTaO_3$ following subsequent irradiation with 91.6 MeV Xe ions utilizing the expression:

$$\chi(n)_{net} = \chi(n)_{df} - \chi(n)_{ps} + \chi(n)_{vg} \quad (1)$$

where $\chi(n)_{df}$, $\chi(n)_{ps}$ and $\chi(n)_{vg}$ are the RBS/C yields measured from a defective (i.e., pre-damaged) region following subsequent irradiation with 91.6 MeV Xe ions, from a pristine region that was irradiated with only 91.6 MeV Xe ions, and from the reference virgin region, respectively. Since disorder production (i.e., ion tracks) is observed in the pristine $KTaO_3$ following irradiation with 91.6 MeV Xe ions, the amount of this disorder should be subtracted from the disorder in pre-damaged $KTaO_3$ following irradiation with SHIs using Eq. (1) in order to accurately evaluate the actual dechanneling fraction. This approach allows better quantitative correlation of ion track dimensions with the amount of pre-damage and was

applied to determine $\chi(n)_{net}$ from the RBS/C spectra provided in Figs. S2b and S2c (supplementary material). Figures 2(a,b) show the fractional Ta disorder with depth extracted from $\chi(n)_{net}$ by the same iterative procedure as above. In this procedure, the dechanneling contribution of disorder in the irradiated crystals is determined and subtracted from $\chi(n)_{net}$ to ascertain the fractional Ta disorder, f_a, with depth for pre-damaged $KTaO_3$ with and without subsequent irradiation with 91.6 MeV Xe ions. By default, this procedure does subtract the background contribution of tracks for a given fluence to the disorder, consistent with Eq. (1) over the whole depth of analysis, and this contribution is accounted for in subsequent analysis below. In the sample with an initial fractional disorder peak, f_0, of ~0.08 (Fig. 2a), the results reveal no significant change, beyond experimental uncertainty, in the disorder profiles of the pre-damaged $KTaO_3$ samples prior to and after 91.6 MeV Xe ion irradiation to 1.0×10^{11} ions/cm^2, which also does not produce significant disorder in the pristine $KTaO_3$ (Fig. S2a) With increase in ion fluence to 1.0×10^{12} ions/cm^2, the relative disorder increases significantly in the pristine sample (Fig. S2a) and in the pre-damage sample (i.e., from ~0.08 to 0.4), both of which agree with the high track densities recorded in the TEM micrographs provided in Fig. S3. In the case of $KTaO_3$ with $f_0 = 0.33$, subsequent irradiation with 91.6 MeV Xe ions to 1.0×10^{11} ions/cm^2 increases the relative disorder from 0.33 to 0.36. Unfortunately, the sample with the highest pre-damage level ($f_0 = 0.33$) and subsequently irradiated with 91.6 MeV Xe ions to 1.0×10^{12} ions/cm^2 exhibited some microcracking on the surface, and thus it was impossible to perform meaningful RBS/C analysis on this sample. Similar cracks have been reported in $BaTiO_3$ irradiated with 635 MeV $^{238}U^+$ ions to 1.4×10^{12} ions/cm^2 and were ascribed to volumetric swelling associated with amorphous tracks or lattice stresses from an irradiation-induced phase transition [57]. Cracking due volume swelling associated with amorphous tracks may explain the observed cracking in the present study, since the density of amorphous tracks and volume swelling should increase with Xe fluence and full

amorphization is expected.

3.2 Thermal spike model results

Figure 3 (a) shows the calculated radial profiles of lattice temperature in $KTaO_3$ with 11% and 30% FPs for thermal spikes corresponding to 18 MeV Si ions, 21 MeV Ni ions and 91.6 MeV Xe ions. In Fig 3 (a), the melting temperature, T_m, of $KTaO_3$ is indicated by a horizontal line. The maximum lattice temperature during the inelastic thermal spike increases with ion energy (i.e., S_e), as illustrated in Fig. 3(a). The lattice temperature depends on both the pre-damage level and the magnitude of the electronic energy loss (S_e). The pre-damage level affects the electron-phonon coupling strength and the heat conductivity, and S_e determines the amount of energy available to transfer to the lattice. The defects increase electron-phonon coupling and, consequently, the profile of energy transferred to the atomic structure [20]. For example, given the same disorder level of 30% FPs, but different energy loss due to 18 MeV Si (green curve) and 91.6 MeV Xe (red curve), the lattice temperature is higher for the higher energy loss, and the heat dissipates within a cylinder along the ion path with larger radius (10 nm vs 15 nm for the 18 MeV Si and 91.6 MeV Xe ions, respectively). As shown in Fig. 3b, the ion track diameter is affected accordingly, and depends on both the pre-damage level and the electronic energy loss. The synergistic effect between the pre-damage and the electronic energy loss depends on the combination of the level of the pre-existing damage and the electronic energy loss.

Figures 3(b-e) show cross-sectional areas (15 nm × 15 nm in size) of the simulation cell at the end of each thermal spike simulation (80 - 180 ps). The track shown in Fig.3(b) is formed in $KTaO_3$ containing 30 % FPs due to a thermal spike corresponding to an 18 MeV Si ion. This is the smallest track obtained, with a diameter of 2.6 ± 0.1 nm, and corresponds to the lowest temperature profile shown in Fig. 3(a). Figures 3(c, d) show the tracks due to thermal spikes, equivalent to 21 MeV Ni ions, in $KTaO_3$ with 11% and 30 % FPs,

respectively; the corresponding track diameters are 3.3 ± 0.2 nm and 5.7 ± 0.2 nm [20]. In Figs. 3(e,f), the amorphous ion tracks due to 91.6 MeV Xe in $KTaO_3$ with 11% and 30 % FPs are shown, with track diameters of 7 ± 0.1 nm and 9.7 ± 0.2 nm, respectively.

4. Discussion

Based on the disorder profiles in Figs. 1 and 2, the dependence of relative Ta disorder, f_a, on fluence in pre-damaged $KTaO_3$ samples irradiated with 18 MeV Si ions or 91.9 MeV Xe ions has been ascertained at several depths (i.e., 50, 75, 100, and 170 nm). The results are shown in Figs. 4 and 5, as a function of ion fluence (ions/nm^2 = 10^{14} ions/cm^2), for 18 MeV Si and 91.6 MeV Xe irradiation, respectively. At each depth, the value of f_a has a minimum value, f_0, that corresponds to the initial pre-damaged level and increases with depth until a maximum value of f_0 is achieved at the damage peak (i.e., 170 nm). Thus, each fit of the direct-impact model (see dash lines in Figs. 4 and 5) has its own f_0 value. As shown in Figs. 4 and 5, the synergistic coupling between electronic energy dissipation from highly ionizing ions with pre-existing damage dramatically enhances damage accumulation in $KTaO_3$. Previous studies of pre-damaged ABO_3 perovskites (e.g. $KTaO_3$ [33,34], $SrTiO_3$ [30], $LiTaO_3$ [58], and $LiNbO_3$ [59,60]) that were subsequently subjected to highly-ionizing ion irradiation have unambiguously established that the growth of any pre-existing defect clusters or amorphous domains due to elastic collisional processes is negligible because of the very low S_n of the ions while traversing the pre-damaged region. Thus, the effects of any collisional-induced defects due to S_n are negligible in this region. In other words, point defect production and aggregation do not contribute to the enhanced damage accumulation observed in $KTaO_3$ (see Figs. 4 and 5). Consequently, the S_e-induced formation of continuous or discontinuous amorphous ion tracks is the primary process responsible for the enhanced disordering rate in $KTaO_3$ with pre-existing damage. It is well established [28,61] that indirect methods (i.e., RBS/C) are more powerful in quantifying the size of discontinuous ion track than direct

observation methods (i.e., TEM), as well as quantifying the size of continuous ion tracks in the presence of high pre-existing damage levels. It should also be mentioned that indirect methods are particularly useful for determining S_e^{th} values, which are difficult to assess by TEM [61] because track radii are often lower than 2 nm for low S_e values and are obscured by the presence of high pre-damage levels, such as in the present study. Therefore, a direct-impact model [62,63] is utilized to describe the increase in relative disorder at constant depth with increasing ion fluence for both 18 MeV Si and 91.6 MeV Xe ions. In this direct-impact description, the amorphous fraction, f_a, at a specific depth from the defect-stimulated component of track formation is given by:

$$f_a = 1 - (1 - f_0) \times \exp(- (\sigma_a - \sigma_p) \times \Phi) \quad (2)$$

where σ_a is the cross-sectional area of the tracks in the pre-damaged region, σ_p is the cross-sectional area of the tracks in pristine $KTaO_3$, which is subtracted in the analysis of RBS/C spectra, Φ is the ion fluence, and f_0 is the initial fractional disorder level in pre-damage $KTaO_3$. Here, σ_p is determined by implementing a direct-impact model to describe the ratio, r, which is the fractional disorder induced in pristine material by ion tracks [40] (discussed in supplementary material) and is therefore given by:

$$r = 1 - \exp(- \sigma_p \times \Phi) \quad (3)$$

If the creation of amorphous latent ion tracks in pristine $KTaO_3$ is disregarded ($\sigma_p = 0$), the amorphous fraction from track formation given by Eq. (2) is simplified [see Eq. (4)].

$$f_a = 1 - (1 - f_0) \times \exp(- \sigma_a \times \Phi) \quad (4)$$

Eq. (4) has been previously used to evaluate the dependence of σ_a on pre-damage level in $KTaO_3$ following 21 MeV Ni ion irradiation [33]; however, that study revealed that no measurable damage was produced in pristine $KTaO_3$, as in the present work for 18 MeV Si ions (see Figs. S1a-c). This is not surprising because the S_e values for both Si (6.16 keV/nm) and Ni (10.16 keV/nm) ions are significantly lower than the recently measured S_e^{th} value for discontinuous track formation in pristine $KTaO_3$ (~13.8 keV/nm) [18]. Thus, in the present study, Eq. (4) is fit to the measured change in disorder with increasing ion fluence for 18 MeV Si ions, as shown in Figs. 4(a,b) by the dashed curves, and the dependence of the derived model parameter, σ_a, on initial disorder level is given in Fig. 4(c). Below an initial disorder levels of 0.35, σ_a exhibits a linear dependence on initial disorder level for 18 MeV Si ions that shows an initial disorder level threshold of 0.1 for track creation under these conditions. which is consistent with the observation of no evidence for synergistic track creation in pre-damaged $KTaO_3$ with an initial peak disorder level of 0.08 and subsequently irradiated with 18 MeV Si ions. The disorder profiles shown in Fig. 1(a) support linear correlation between σ_a and initial disorder. The initial disorder level threshold of 0.1 for creation of tracks in $KTaO_3$ with 18 MeV Si ions is larger than that previously reported for $KTaO_3$ irradiated with 21 Ni ions (0.03) [33]. This finding unambiguously establishes that the threshold disorder level for track formation in $KTaO_3$ increases with decreasing values of S_e for incident ions. A similar linear correlation between σ_a and initial disorder has been previously observed in $SrTiO_3$ [30]. In previous MD simulations [32,34], it has been shown that this linear increase in σ_a with initial disorder is consistent with increases in electron-phonon coupling and decreases in thermal conductivity due increased electron and phonon scattering from the defects. Consequently, the radial thermal spike profile is notably affected, which directly influences the depth dependence of amorphous track size. The current MD simulations validate the track

sizes, determined by an indirect method (i.e., RBS/C), in pre-damaged $KTaO_3$ irradiated with 18 MeV Si ions.

Wesch et al. [64,65] and Kamarou et al. [66–69] have previously reported on SHI irradiation effects in pristine semiconductors and showed that the ratio, *r*, at depths beyond a narrow surface layer (tens of nanometer) is nearly constant. This indicates that the track size is relatively uniform for a nearly constant S_e over a large depth region. These studies suggested that the thin surface layer remains almost undamaged because the charge state of the incident ion is significantly less than the mean equilibrium charge state in the sample, and *r* was determined only at one depth behind the undamaged narrow surface layer [67,68]. Thus, in this study, the values of *r* in pristine $KTaO_3$ were determined from the RBSC spectra (Fig. S2) at a depth of 70 nm using the Kamarou et al. method [68,69], and the dependence of *r* on 91.6 MeV Xe ion fluence is given in Fig. 5(a). The particulars of this analysis are provided in the supplementary material. Furthermore, Eq. (3) has been fit to the increase in *r* with fluence in Fig. 5(a), and the value of σ_p for 91.6 MeV Xe ions in pristine $KTaO_3$ was determined. This cross section, σ_p, for track formation in pristine materials is used in Eq. (2) to fit the change in disorder in pre-damaged $KTaO_3$ with increasing Xe ion fluence, as illustrated in Figs. 5(b,c), where the dashed curves represent the best fits of Eqs. (2) and (3) to the data, which yield σ_a. Considering a nearly circular amorphous cross-section, an equivalent ion track diameter, *d*, is given by:

$$d^2 = 4\sigma_a/\pi \quad (5)$$

The properties and conditions for track formation in pre-damaged $KTaO_3$ at 300 K are now discussed in more detail. The effective track diameters as functions of initial disorder for 18 MeV Si and 91.6 MeV Xe ions in $KTaO_3$ are illustrated in Fig. 6(a); along with data for 21

MeV Ni ions [33]. The curves in Fig. 6 are just polynomial or spline fits to the data. In $KTaO_3$ with an initial disorder level of f_0 = 0.33, the tracks formed by irradiation with 18 MeV Si ions, have an average diameter of 2.7 ± 0.3 nm. This experimentally determined track diameter is consistent with that obtained from MD simulations (2.6 ± 0.1 nm for 30 % FPs). With an increase in level of pre-existing disorder to f_0 = 0.53 in $KTaO_3$, the average diameter of the tracks due to 18 MeV Si ions increases to 5.9 ± 0.6 nm. Similar to the 18 MeV Si irradiation, an increase of ion track diameter with increasing pre-existing disorder level has been reported for 21 MeV Ni ions [33], and the experimentally determined track diameters for 91.6 MeV Xe ions are 3.3 ± 0.2 nm, 8.0 ± 0.4 nm, and 14.3 ± 0.7 nm, for initial disorder levels, f_0, of 0.0, 0.08 and 0.33, respectively. While there is some difference in the ion fluxes for these ions, the ion fluxes ($< 6\times10^{10}$ ions/cm^2·s) are not expected to increase the temperature or affect track size. The MD simulations reveal that for increasing pre-existing damage level, the lattice temperature within the thermal spike increases because the defects increase the electron-phonon coupling leading to more radially confined energy dissipation to the lattice, as shown in Fig.3(a). In general, higher temperatures form larger track sizes [4]. The results further show that, for low levels of initial disorder, track size exhibits a linear relationship with the pre-existing disorder level in $KTaO_3$. As the initial disorder level increases in $KTaO_3$, the track diameters tend to saturate, which agrees with previous results obtained at 300 K for 21 MeV Ni ions [33] and previous MD simulations [32]. For the same initial disorder level, the results in Fig. 6(a) reveal that smaller average track sizes are created for 18 MeV Si ions than for either 21 MeV Ni and 91.6 MeV Xe ions. In other words, the average track size increases as S_e increases, which is consistent with the increasing thermal-spike temperature with increasing S_e, as observed in the MD simulations.

To better highlight this effect, track cross sections for pristine and defective $KTaO_3$, irradiated with Si, Ni and Xe ions, are depicted versus S_e in Fig. 6(b), along with results for

358 MeV Ni ion irradiation of pristine $KTaO_3$ [18]. Note that the value of f_0 is labeled for each irradiation condition in Fig. 6(b). As shown in Fig. 6(b), for pristine $KTaO_3$ ($f_0 = 0.0$) and for a low initial peak disorder level ($f_0 = 0.08$), the measured track cross sections increase linearly with S_e. With an increase in level of pre-existing disorder to $f_0 = 0.33$ in $KTaO_3$, the track cross section increases linearly for S_e values below 10 keV/nm, but tends to saturate for higher S_e values. As evidenced in Fig. 6(b), no tracks are detected in pristine $KTaO_3$ irradiated with ions having S_e less than 10 keV/nm (i.e. 21 MeV Ni ions); whereas swift heavy ions (e.g., 91.6 MeV Xe ions) produce ion tracks in pristine $KTaO_3$. It has been reported that S_e values above 12.0 keV/nm may be required to form ion tracks in pristine $KTaO_3$ [18]. The threshold value, S_e^{th}, for track creation at different pre-damage levels can be extracted from the results in Fig 6(b), and the values of S_e^{th} are provided in Fig. 6(c) as a function of initial level of disorder. It is obvious that the value of S_e^{th} shifts to higher values with decreasing initial disorder level. For example, while a minimum value of S_e^{th} is achieved for a high initial disorder level (i.e., ~5.02 keV/nm for $f_0 = 0.53$), a maximum value is achieved for pristine $KTaO_3$ (i.e., ~10.81 keV/nm for $f_0 = 0.0$). It is also striking to note that the value of S_e^{th} decreases slowly from 6.68 keV/nm to 5.02 keV/nm as f_0 increases from 0.08 to 0.53, respectively; while on the other hand, S_e^{th} increases rapidly for f_0 values below 0.08, up to a value of 10.81 keV/nm for pristine $KTaO_3$. These results indicate that this synergistic track formation has a strong dependence on both the initial level of pre-damage in $KTaO_3$ and the values of S_e for the incident ions. Experimental [70,71] and theoretical [72] studies have determined that for the same values of S_e, measured track radii are larger in the low velocity regime than in the high velocity regime [73]. Although similar dependencies are predicted for $KTaO_3$ [18], additional studies are required for a comprehensive understanding of the relationship between S_e^{th} and ion velocity.

As aforementioned, the current MD simulations validate the observed trends for experimentally determined track sizes in pre-damaged $KTaO_3$ irradiated with highly ionizing ions. An example is provided in Fig. 7, which compares the track sizes determined via RBS/C and MD in pre-damaged $KTaO_3$ with an initial disorder level of f_0 = 0.33 and 30 % preexisting FPs, respectively. The MD results confirm that the track size increases linearly for S_e values below 10 keV/nm, but tends to saturate for higher Se values. However, this comparison indicates that the experimentally determined track sizes are larger compared to the ones determined by MD. As discussed previously [34], the main sources of this discrepancy are the estimated values of the e-ph coupling parameter and an inaccurate correlation between disorder (measured by ion channeling) and the MD FP concentration. Additionally, the ion channeling measurements determine an average size of a large number of tracks, while the MD values are an average of measurements along one track.

Finally, this study reveals that a threshold disorder level above 0.08 (i.e., 0.1) is required to stimulate track formation in pre-damaged $KTaO_3$ with 18 MeV Si ions (see Fig. 4c). Below this value, an equilibrium between damage recovery and damage production processes is observed (see Fig .1a). In other word, the synergistic effect is not active. These findings indicate the existence of two processes for a low initial damage level ($f_0 \sim 0.10$): (1) $S_e > 6.16$ keV/nm, where the synergistic effect is active, and (2) $S_e < 6.16$ keV/nm, where athermal annealing from the thermal spike associated with S_e competes with damage production. Highly ionizing ions with $S_e < 6.16$ keV/nm may promote defect recovery in $KTaO_3$ by enhancing the mobility of point defects via thermal spikes that do not achieve melting or ionization-induced diffusion [74], as observed in $SrTiO_3$ [56]. A more quantitative understanding of these processes requires additional investigation of this competitive (recovery) effect on defect production and evolution in defective $KTaO_3$.

5. Conclusions

Improved understanding and advanced models of electronic energy loss (S_e) effects on ion track creation in defective solids may provide new pathways to control ion track creation and properties and thus more flexibility to tailor properties and functionalities of complex oxides for a range of applications. In this regard, the synergy of pre-existing damage states with the dissipation of S_e from highly ionizing ions has been studied for single crystal $KTaO_3$. The results demonstrate that this synergistic interaction enhances formation of amorphous ion tracks, and the dimensions of these amorphous tracks exhibit a strong dependence on S_e and the level of pre-existing disorder. The results further reveal the threshold values, S_e^{th}, for this synergistic effect and their dependence on pre-damage level, which was the research goal. The values of S_e^{th} increase from 5.02 keV/nm for a pre-existing fractional disorder of 0.53 to 6.68 keV/nm for a pre-existing fractional disorder level of 0.08 and to 10.81 keV/nm for pristine $KTaO_3$. Above these thresholds, amorphous latent tracks are produced due to local melting and rapid quenching processes. Below a disorder fraction of 0.08 and $S_e \leq 6.68$ keV/nm, this synergistic effect is not active and may in fact be in equilibrium with a damage annealing process. While there is no evidence for ion track creation in pristine $KTaO_3$ for ions with $S_e < 10$ keV/nm, swift heavy ions with $S_e > 11$ keV/nm (e.g., 91.6 MeV Xe ions) create ion tracks in pristine $KTaO_3$. Moreover, for a given level of pre-existing damage, the average track size increases with S_e. These findings indicate that it is possible to tune track size and location in a material by selective control of initial pre-damaged level and the electronic energy loss deposited by highly ionizing ions.

Acknowledgements

The work performed by the researchers in Romania was supported by a grant of the Romanian Ministry of Education and Research, CNCS – UEFISCDI, project number PN-III-P4-ID-PCE2020-1379, within PNCDI III. Use of the 3 MV Tandetron Cockcroft-Walton accelerator at IFIN-HH was financially supported by the Romanian Governmental Programme through the National Programme "Instalatii si Obiective de Interes National". The Au ion irradiations

to pre-damage samples for the Xe irradiations, the characterization of the Xe-irradiated samples and the MD simulations were supported by the U.S. Department of Energy, Office of Science, Basic Energy Sciences, Materials Sciences and Engineering Division under contract number DE-AC05-00OR22725. The MD simulations used resources of the National Energy Research Scientific Computing Center, supported by the Office of Science, U.S. Department of Energy under Contract No. DEAC02-05CH11231. The Xe irradiations were performed at the IRRSUD beamline of the Grand Accélérateur National d'Ions Lourds (GANIL), Caen, France and the authors thank the CIMAP, CIRIL and GANIL technical staff.

References

[1] Colligon J 1986 Surface modification by ion beams *Vacuum* **36** 413–8

[2] Nastasi M A and Mayer J W 2006 *Ion implantation and synthesis of materials* (Springer-Verlag)

[3] Agulló-López F, Climent-Font A, Muñoz-Martín Á, Olivares J and Zucchiatti A 2016 Ion beam modification of dielectric materials in the electronic excitation regime: Cumulative and exciton models *Prog. Mater. Sci.* **76** 1–58

[4] Wesch W and Wendler E 2016 *Ion beam modification of solids : ion-solid interaction and radiation damage*

[5] Zhang Y and Weber W J 2020 Ion irradiation and modification: The role of coupled electronic and nuclear energy dissipation and subsequent nonequilibrium processes in materials *Appl. Phys. Rev.* **7** 041307

[6] Karlušić M, Mičetić M, Kresić M, Jakšić M, Šantić B, Bogdanović-Radović I, Bernstorff S, Lebius H, Ban-d'Etat B, Žužek Rožman K, O'Connell J H, Hagemann U and Schleberger M 2020 Nanopatterning surfaces by grazing incidence swift heavy ion irradiation *Appl. Surf. Sci.* 148467

[7] Elliman R G and Williams J S 2015 Advances in ion beam modification of semiconductors *Curr. Opin. Solid State Mater. Sci.* **19** 49–67

[8] Wang X, Wan W, Shen S, Wu H, Zhong H, Jiang C and Ren F 2020 Application of ion beam technology in (photo)electrocatalytic materials for renewable energy *Appl. Phys. Rev.* **7** 41303

[9] Anon 2000 *Defects and Surface-Induced Effects in Advanced Perovskites* (Springer Netherlands)

[10] Bazzan M and Sada C 2015 Optical waveguides in lithium niobate: Recent developments and applications *Appl. Phys. Rev.* **2** 40603

[11] Harashima S, Bell C, Kim M, Yajima T, Hikita Y and Hwang H Y 2013 Coexistence of two-dimensional and three-dimensional Shubnikov–de Haas oscillations in Ar + -irradiated KTaO 3 *Phys. Rev. B* **88** 085102

[12] Wadehra N, Tomar R, Halder S, Sharma M, Singh I, Jena N, Prakash B, De Sarkar A, Bera C, Venkatesan A and Chakraverty S 2017 Electronic structure modification of the KTaO 3 single-crystal surface by Ar + bombardment *Phys. Rev. B* **96** 115423

[13] Gentils A, Copie O, Herranz G, Fortuna F, Bibes M, Bouzehouane K, Jacquet É, Carrétéro C, Basletić M, Tafra E, Hamzić A and Barthélémy A 2010 Point defect distribution in high-mobility conductive SrTiO 3 crystals *Phys. Rev. B* **81** 144109

[14] Herranz G, Copie O, Gentils A, Tafra E, Basletić M, Fortuna F, Bouzehouane K, Fusil S, Jacquet É, Carŕtro C, Bibes M, Hamzić A and Barthĺmy A 2010 Vacancy defect and carrier distributions in the high mobility electron gas formed at ion-irradiated SrTiO3 surfaces *J. Appl. Phys.* **107**

[15] Wang Q, Zhang W, Zhang W and Zeng H 2016 In-situ monitor of insulator to metal transition in SrTiO 3 by Ar + irradiation *Appl. Surf. Sci.* **365** 84–7

[16] Pennycook T J, Beck M J, Varga K, Varela M, Pennycook S J and Pantelides S T 2010 Origin of colossal ionic conductivity in oxide multilayers: Interface induced sublattice disorder *Phys. Rev. Lett.* **104** 115901

[17] Wong J Y C, Zhang L, Kakarantzas G, Townsend P D, Chandler P J and Boatner L A 1992 Ion-implanted optical waveguides in KTaO $_3$ *J. Appl. Phys.* **71** 49–52

[18] Han X, Liu Y, Huang Q, Crespillo M L, Liu P and Wang X 2020 Swift heavy ion tracks in alkali tantalate crystals: a combined experimental and computational study *J. Phys. D. Appl. Phys.* **53** 105304

[19] Pea-Rodrguez O, Olivares J, Carrascosa M, Garca-Cabaes ngel, Rivera A and Agull-Lpez F 2012 Optical Waveguides Fabricated by Ion Implantation/Irradiation: A Review Optical Waveguides Fabricated by Ion Implantation/Irradiation: A Review *Ion Implantation* (InTech)

[20] Ueno K, Inoue I H, Yamada T, Akoh H, Tokura Y and Takagi H 2004 Field-effect transistor based on KTaO3 perovskite *Appl. Phys. Lett.* **841**

[21] Ueno K, Nakamura S, Shimotani H, Yuan H T, Kimura N, Nojima T, Aoki H, Iwasa Y and Kawasaki M 2011 Discovery of superconductivity in KTaO3 by electrostatic carrier doping *Nat. Nanotechnol.* **6** 408–12

[22] Prassides K 2011 Superconductivity at the double *Nat. Nanotechnol.* **6** 400–1

[23] Meldrum A, Boatner L . and Ewing R . 1998 Effects of ionizing and displacive irradiation on several perovskite-structure oxides *Nucl. Instruments Methods Phys. Res. Sect. B Beam Interact. with Mater. Atoms* **141** 347–52

[24] Meldrum A, Boatner L A, Weber W J and Ewing R C 2002 Amorphization and recrystallization of the ABO3 oxides *J. Nucl. Mater.* **300** 242–54

[25] Velişa G, Wendler E, Wang L-L, Zhang Y and Weber W J 2019 Ion mass dependence of irradiation-induced damage accumulation in KTaO3 *J. Mater. Sci.* **54** 149–58

[26] Wong J Y C, Zhang L, Kakarantzas G, Townsend P D, Chandler P J and Boatner L A 1992 Ion-implanted optical waveguides in KTaO3 *J. Appl. Phys.* **71** 49–52

[27] Weber W J, Jiang W, Thevuthasan S, Williford R E, Meldrum A and Boatner L A 2000 Ion-Beam-Induced Defects and Defects Interactions in Perovskite-Structure Titanates *Defects and Surface-Induced Effects in Advanced Perovskites* (Dordrecht: Springer Netherlands) pp 317–28

[28] Lang M, Djurabekova F, Medvedev N, Toulemonde M and Trautmann C 2020 Fundamental Phenomena and Applications of Swift Heavy Ion Irradiations *Reference Module in Materials Science and Materials Engineering* (Elsevier)

[29] Karlušić M, Jakšić M, Lebius H, Ban-d'Etat B, Wilhelm R A, Heller R and Schleberger M 2017 Swift heavy ion track formation in SrTiO 3 and TiO 2 under random, channeling and near-channeling conditions *J. Phys. D. Appl. Phys.* **50** 205302

[30] Xue H, Zarkadoula E, Liu P, Jin K, Zhang Y and Weber W J 2017 Amorphization due to electronic energy deposition in defective strontium titanate *Acta Mater.* **127** 400–6

[31] Weber W J, Zarkadoula E, Pakarinen O H, Sachan R, Chisholm M F, Liu P, Xue H, Jin K and Zhang Y 2015 Synergy of elastic and inelastic energy loss on ion track

formation in SrTiO3. *Sci. Rep.* **5** 7726

[32] Zarkadoula E, Jin K, Zhang Y and Weber W J 2017 Synergistic effects of nuclear and electronic energy loss in $KTaO_3$ under ion irradiation *AIP Adv.* **7** 015016

[33] Jin K, Zhang Y and Weber W J 2018 Synergistic effects of nuclear and electronic energy deposition on damage production in $KTaO_3$ *Mater. Res. Lett.* **6** 531–6

[34] Zarkadoula E, Zhang Y and Weber W J 2020 Molecular dynamics simulations of the response of pre-damaged SrTiO3 and KTaO3 to fast heavy ions *AIP Adv.* **10** 015019

[35] Jubera M, Villarroel J, García-Cabañes A, Carrascosa M, Olivares J, Agullo-López F, Méndez A and Ramiro J B 2012 Analysis and optimization of propagation losses in LiNbO3 optical waveguides produced by swift heavy-ion irradiation *Appl. Phys. B* **107** 157–62

[36] Ashkin A, Boyd G D, Dziedzic J M, Smith R G, Ballman A A, Levinstein J J and Nassau K 1966 Optically-induced refractive index inhomogeneities in LiNbO3 and LiTaO3 *Appl. Phys. Lett.* **9** 72–4

[37] Liu G, He R, Akhmadaliev S, Vázquez De Aldana J R, Zhou S and Chen F 2014 Optical waveguides in LiTaO3 crystals fabricated by swift C 5+ ion irradiation *Nucl. Instruments Methods Phys. Res. Sect. B Beam Interact. with Mater. Atoms* **325** 43–6

[38] Yamaichi E, Watanabe K, Imamiya K and Ohi K 1987 Photoluminescence in KTaO3 Single Crystal *J. Phys. Soc. Japan* **56** 1890–7

[39] Waiblinger M, Sommerhalter C, Pietzak B, Krauser J, Mertesacker B, Lux-Steiner M C, Klaumünzer S, Weidinger A, Ronning C and Hofsäß H 1999 Electrically conducting ion tracks in diamond-like carbon films for field emission *Appl. Phys. A Mater. Sci. Process.* **69** 239–40

[40] Xue H, Zarkadoula E, Sachan R, Zhang Y, Trautmann C and Weber W J 2018 Synergistically-enhanced ion track formation in pre-damaged strontium titanate by energetic heavy ions *Acta Mater.* **150** 351–9

[41] Burducea I, Straticiuc M, Ghiță D G, Moșu D V, Călinescu C I, Podaru N C, Mous D J W, Ursu I and Zamfir N V 2015 A new ion beam facility based on a 3 MV Tandetron™ at IFIN-HH, Romania *Nucl. Instruments Methods Phys. Res. Sect. B Beam Interact. with Mater. Atoms* **359** 12–9

[42] Zhang Y, Lian J, Zhu Z, Bennett W D, Saraf L V, Rausch J L, Hendricks C A, Ewing R C and Weber W J 2009 Response of strontium titanate to ion and electron irradiation *J. Nucl. Mater.* **389** 303–10

[43] Zhang Y, Crespillo M L, Xue H, Jin K, Chen C H, Fontana C L, Graham J T and Weber W J 2014 New ion beam materials laboratory for materials modification and irradiation effects research *Nucl. Instruments Methods Phys. Res. Sect. B Beam Interact. with Mater. Atoms* **338** 19–30

[44] Ziegler J F and Biersack J P 1985 The Stopping and Range of Ions in Matter *Treatise on Heavy-Ion Science* (Boston, MA: Springer US) pp 93–129

[45] Weber W J and Zhang Y 2019 Predicting damage production in monoatomic and multi-elemental targets using stopping and range of ions in matter code: Challenges and recommendations *Curr. Opin. Solid State Mater. Sci.* **23** 100757

[46] Toulemonde M, Assmann W, Dufour C, Medd A M-M F and 2006 undefined Experimental phenomena and thermal spike model description of ion tracks in amorphisable inorganic insulators

[47] Todorov I T, Smith W, Trachenko K and Dove M T 2006 DL_POLY_3: New dimensions in molecular dynamics simulations via massive parallelism *J. Mater. Chem.* **16** 1911–8

[48] McCoy M A, Grimes R W and Lee W E 1997 Phase stability and interfacial structures in the Sr0-SrTiO3system *Philos. Mag. A Phys. Condens. Matter, Struct. Defects Mech.*

Prop. **75** 833–46
[49] I. T. Todorov and W. Smith T No Title *he DL Poly 4 User Manual, v. 4, Www.ccp5. (2012)., Ac.uk/DL_POLY/MANUALS/USRMAN4.pdf*
[50] Rao S I and Houska C R 1990 Residual stress gradients along ion implanted zones ? cubic crystals *J. Mater. Sci.* **25** 2822–6
[51] Turos A, Gaca J, Wojcik M, Nowicki L, Ratajczak R, Groetzschel R, Eichhorn F and Schell N 2004 Virtues and pitfalls in structural analysis of compound semiconductors by the complementary use of RBS/channeling and high resolution X-ray diffraction *Nucl. Instruments Methods Phys. Res. Sect. B Beam Interact. with Mater. Atoms* **219–220** 618–25
[52] Decoster S and Vantomme A 2009 *Implantation-induced damage in Ge: strain and disorder profiles during defect accumulation and recovery* vol 42 (IOP Publishing)
[53] Debelle A, Boulle A, Rakotovao F, Moeyaert J, Bachelet C, Garrido F and Thomé L 2013 Influence of elastic properties on the strain induced by ion irradiation in crystalline materials *J. Phys. D. Appl. Phys.* **46** 045309
[54] Mejai N, Debelle A, Thomé L, Sattonnay G, Gosset D, Boulle A, Dargis R and Clark A 2015 Depth-dependent phase change in Gd_2O_3 epitaxial layers under ion irradiation *Appl. Phys. Lett.* **107** 131903
[55] Velişa G, Wendler E, Xue H, Zhang Y and Weber W J 2018 Revealing ionization-induced dynamic recovery in ion-irradiated SrTiO 3 *Acta Mater.* **149** 256–64
[56] Weber W J, Xue H, Zarkadoula E and Zhang Y 2019 Two regimes of ionization-induced recovery in SrTiO3 under irradiation *Scr. Mater.* **173** 154–7
[57] Jiang W, Devanathan R, Sundgren C J, Ishimaru M, Sato K, Varga T, Manandhar S and Benyagoub A 2013 Ion tracks and microstructures in barium titanate irradiated with swift heavy ions: A combined experimental and computational study *Acta Mater.* **61** 7904–16
[58] Sellami N, Crespillo M L, Zhang Y and Weber W J 2018 Two-stage synergy of electronic energy loss with defects in $LiTaO_3$ under ion irradiation *Mater. Res. Lett.* **6** 339–44
[59] Liu P, Zhang Y, Xue H, Jin K, Crespillo M L, Wang X and Weber W J 2016 A coupled effect of nuclear and electronic energy loss on ion irradiation damage in lithium niobate *Acta Mater.* **105** 429–37
[60] Sellami N, Crespillo M L, Xue H, Zhang Y and Weber W J 2017 Role of atomic-level defects and electronic energy loss on amorphization in LiNbO3 single crystals *J. Phys. D. Appl. Phys.* **50** 325103
[61] Thomé L 2016 Swift heavy ion irradiation of crystalline insulators and metals *Springer Series in Surface Sciences* vol 61 (Springer Verlag) pp 321–63
[62] Gibbons J F 1972 Ion implantation in semiconductors—Part II: Damage production and annealing *Proc. IEEE* **60** 1062–96
[63] Weber W . 2000 Models and mechanisms of irradiation-induced amorphization in ceramics *Nucl. Instruments Methods Phys. Res. Sect. B Beam Interact. with Mater. Atoms* **166–167** 98–106
[64] Wesch W, Kamarou A, Wendler E, Gärtner K, Gaiduk P I and Klaumünzer S 2003 Ionisation stimulated defect annealing in GaAs and InP *Nuclear Instruments and Methods in Physics Research, Section B: Beam Interactions with Materials and Atoms* vol 206 (North-Holland) pp 1018–23
[65] Wesch W, Kamarou A and Wendler E 2004 Effect of high electronic energy deposition in semiconductors *Nucl. Instruments Methods Phys. Res. Sect. B Beam Interact. with Mater. Atoms* **225** 111–28
[66] Kamarou A, Wesch W, Wendler E and Klaumünzer S 2004 Damage formation and

annealing in InP due to swift heavy ions *Nuclear Instruments and Methods in Physics Research, Section B: Beam Interactions with Materials and Atoms* vol 225 (North-Holland) pp 129–35

[67] Kamarou A, Wendler E and Wesch W 2005 Charge state effect on near-surface damage formation in swift heavy ion irradiated InP *J. Appl. Phys.* **97** 123532

[68] Kamarou A, Wesch W, Wendler E, Undisz A and Rettenmayr M 2006 Swift heavy ion irradiation of InP: Thermal spike modeling of track formation *Phys. Rev. B - Condens. Matter Mater. Phys.* **73** 184107

[69] Kamarou A, Wesch W, Wendler E, Undisz A and Rettenmayr M 2008 Radiation damage formation in InP, InSb, GaAs, GaP, Ge, and Si due to fast ions *Phys. Rev. B - Condens. Matter Mater. Phys.* **78** 054111

[70] Meftah A, Brisard F, Costantini J M, Hage-Ali M, Stoquert J P, Studer F and Toulemonde M 1993 Swift heavy ions in magnetic insulators: A damage-cross-section velocity effect *Phys. Rev. B* **48** 920–5

[71] Karlušić M, Ghica C, Negrea R F, Siketić Z, Jakšić M, Schleberger M and Fazinić S 2017 On the threshold for ion track formation in CaF2 *New J. Phys.* **19** 023023

[72] Szenes G 2020 Materials parameters and ion-induced track formation *Radiat. Eff. Defects Solids* **175** 241–56

[73] Meftah A, Costantini J M, Khalfaoui N, Boudjadar S, Stoquert J P, Studer F and Toulemonde M 2005 Experimental determination of track cross-section in Gd3Ga 5O12 and comparison to the inelastic thermal spike model applied to several materials *Nucl. Instruments Methods Phys. Res. Sect. B Beam Interact. with Mater. Atoms* **237** 563–74

[74] Zinkle S J, Skuratov V A and Hoelzer D T 2002 On the conflicting roles of ionizing radiation in ceramics *Nucl. Instruments Methods Phys. Res. Sect. B Beam Interact. with Mater. Atoms* **191** 758–66

[75] Wendler E, Schilling M and Wendler L 2014 Low-temperature damage formation in ion-implanted SiC and its correlation with primary energy deposition *Vacuum* **105** 102–6

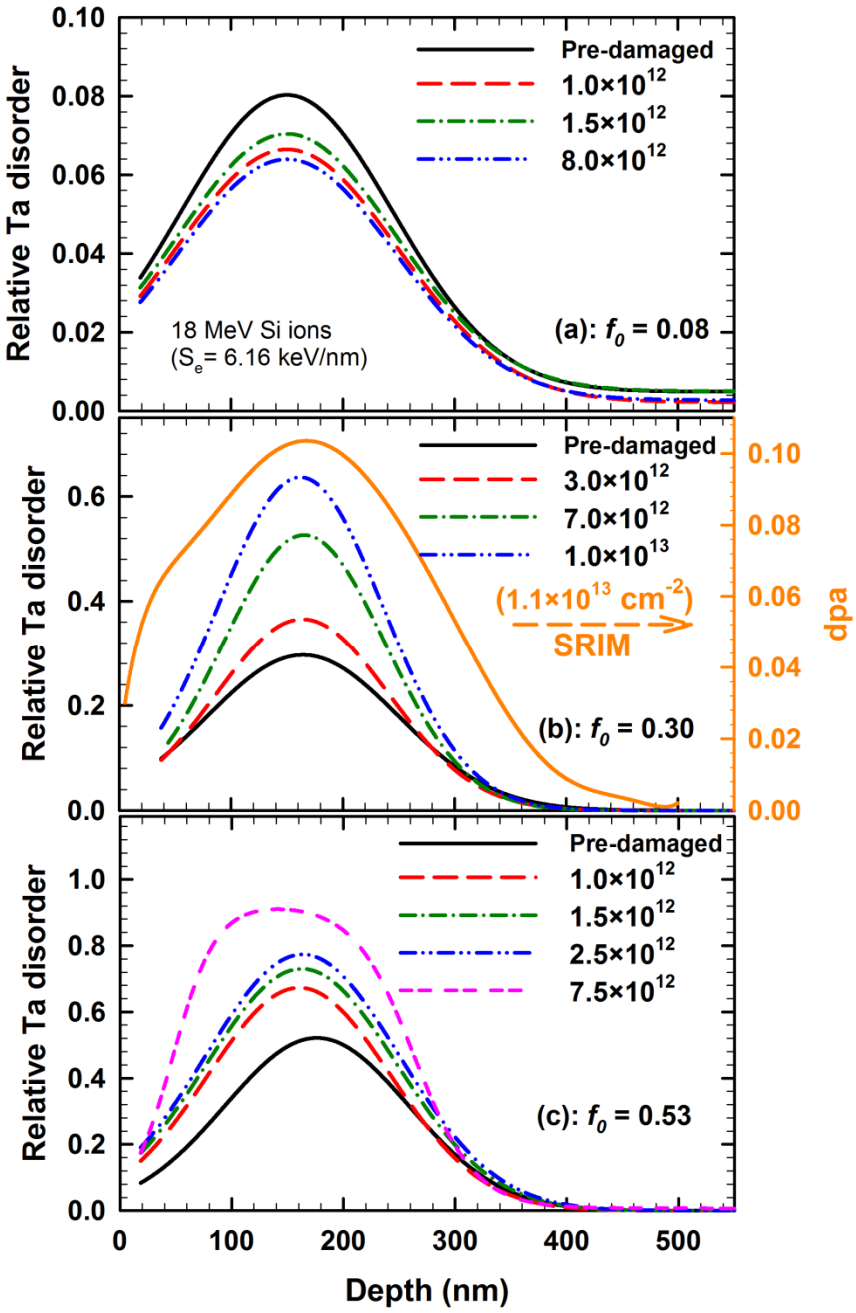

Fig.1. Relative Ta disorder as a function of depth for pre-damaged $KTaO_3$ irradiated with 18 MeV Si ions at 300 K to different ion fluences: (a) maximum initial disorder fraction $f_0 = 0.08$; (b) $f_0 = 0.30$ and (c) $f_0 = 0.53$. In (b), the SRIM-derived damage dose (dpa) profile (right axis) for a fluence of 1.1×10^{13} Au ions/cm^2, is included for comparison. The experiment uncertainty for the curves is estimated to be ~15%, which is mainly attributed to the statistics of the backscattering spectra [75] and to the standard deviation in fitting the experimental disorder profiles.

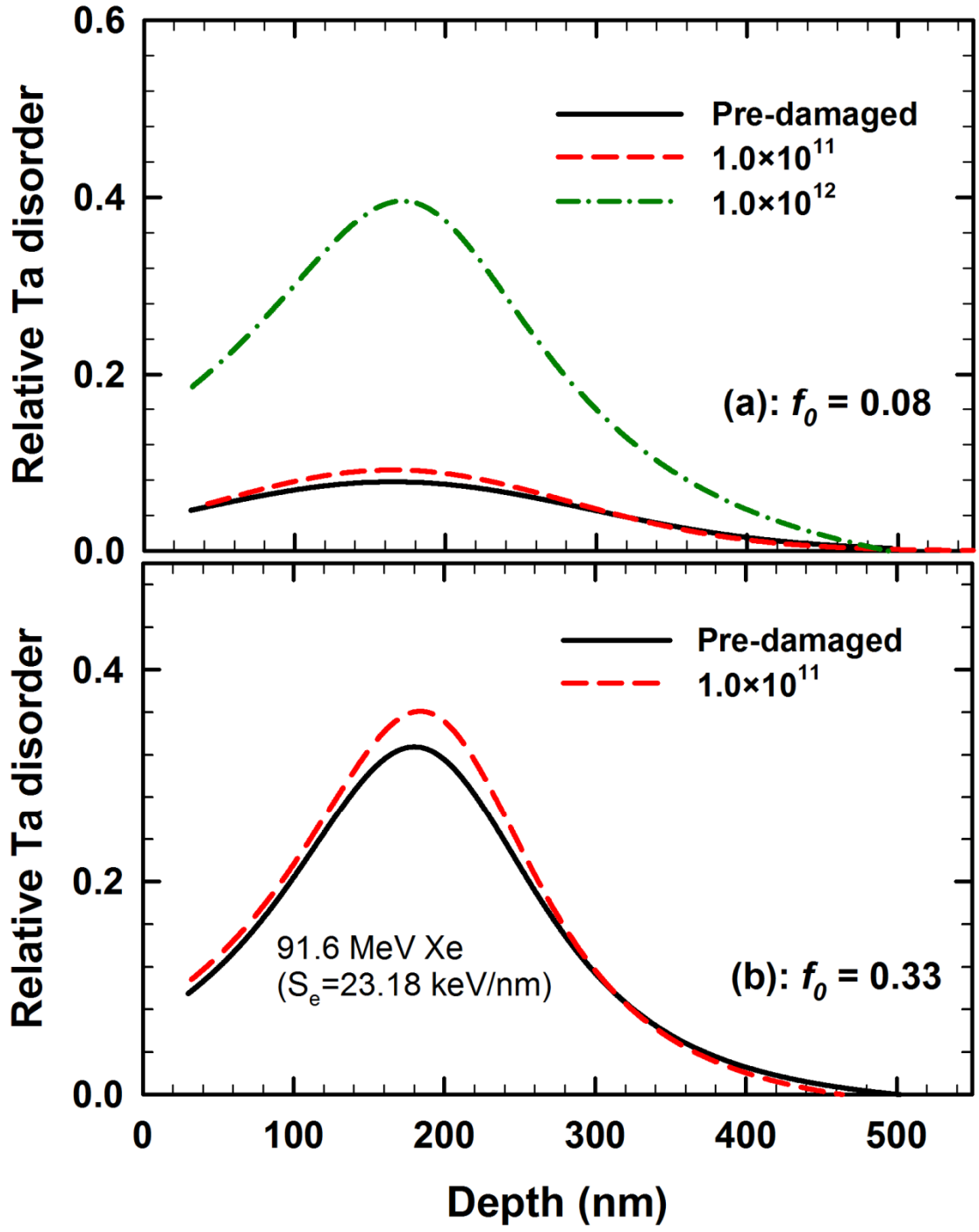

Fig. 2. Relative Ta disorder as a function of depth for pre-damaged $KTaO_3$ irradiated with 91.6 MeV Xe ions at 300 K to different fluences: (a) maximum initial disorder fraction f_0 = 0.08 and (b) f_0 = 0.33. The experiment uncertainty is estimated to be ~ 15%, which is mainly attributed to the statistics of the backscattering spectra [51] and to the standard deviation in fitting the experimental disorder profiles.

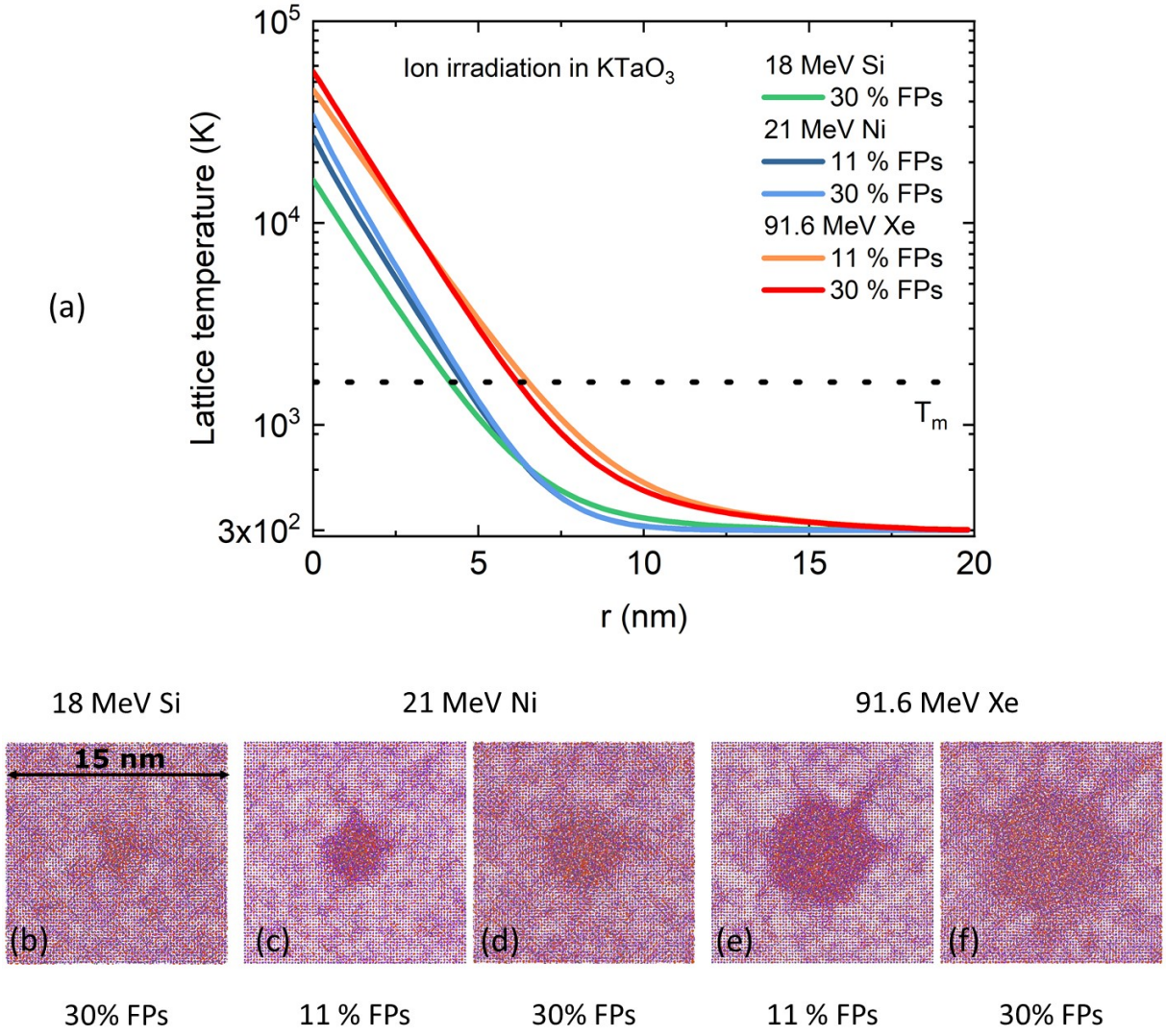

Fig. 3. (a) Radial profiles of lattice temperature in $KTaO_3$ with 11 % and 30 % pre-existing Frenkel pairs for ions and energies in this study. (b-f) Cross sections of the irradiated systems at the end of each simulation, at times 180 ps, 80 ps, 98 ps, 100 ps, and 112 ps, respectively. All cross-sectional areas shown have size 15 × 15 nm. K atoms are shown in red, Ta atoms in grey and O atoms in purple.

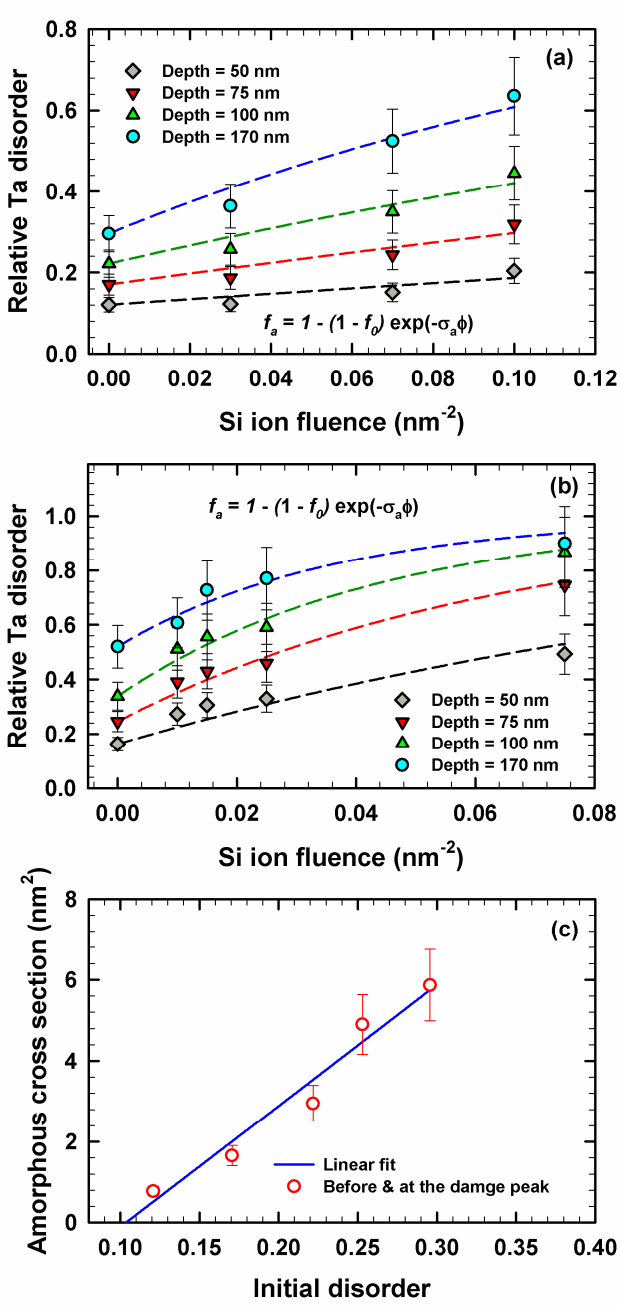

Fig. 4. Relative Ta disorder in pre-damaged $KTaO_3$ as a function of Si ion fluence (ions/nm^2 = 10^{14} ions/cm^2) at different depths, along with curve fits of direct-impact model (Eq. 4): (a) maximum initial disorder fraction f_0 = 0.30 and (b) f_0 = 0.53. (c) Dependence of amorphous cross-section on initial level of disorder in $KTaO_3$.

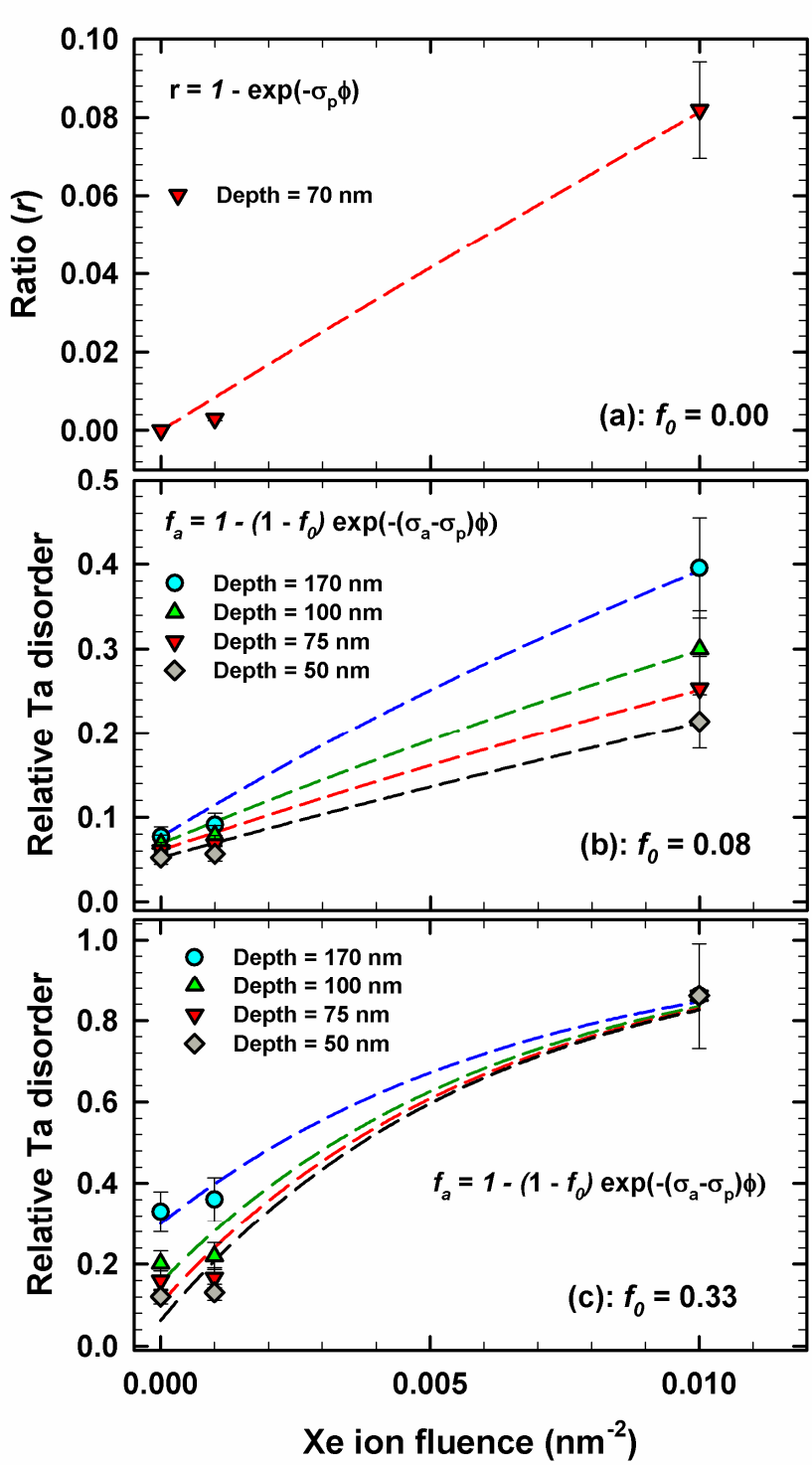

Fig. 5. Relative Ta disorder in $KTaO_3$ as a function of Xe ion fluence (ions/nm^2 = 10^{14} ions/cm^2) at different depths: (a) pristine or f_0 = 0.00, (b) f_0 = 0.08 and (c) f_0 = 0.33. Eq. (3) has been fit to data in (a), while Eq. (2) has fit to data in (b) and (c).

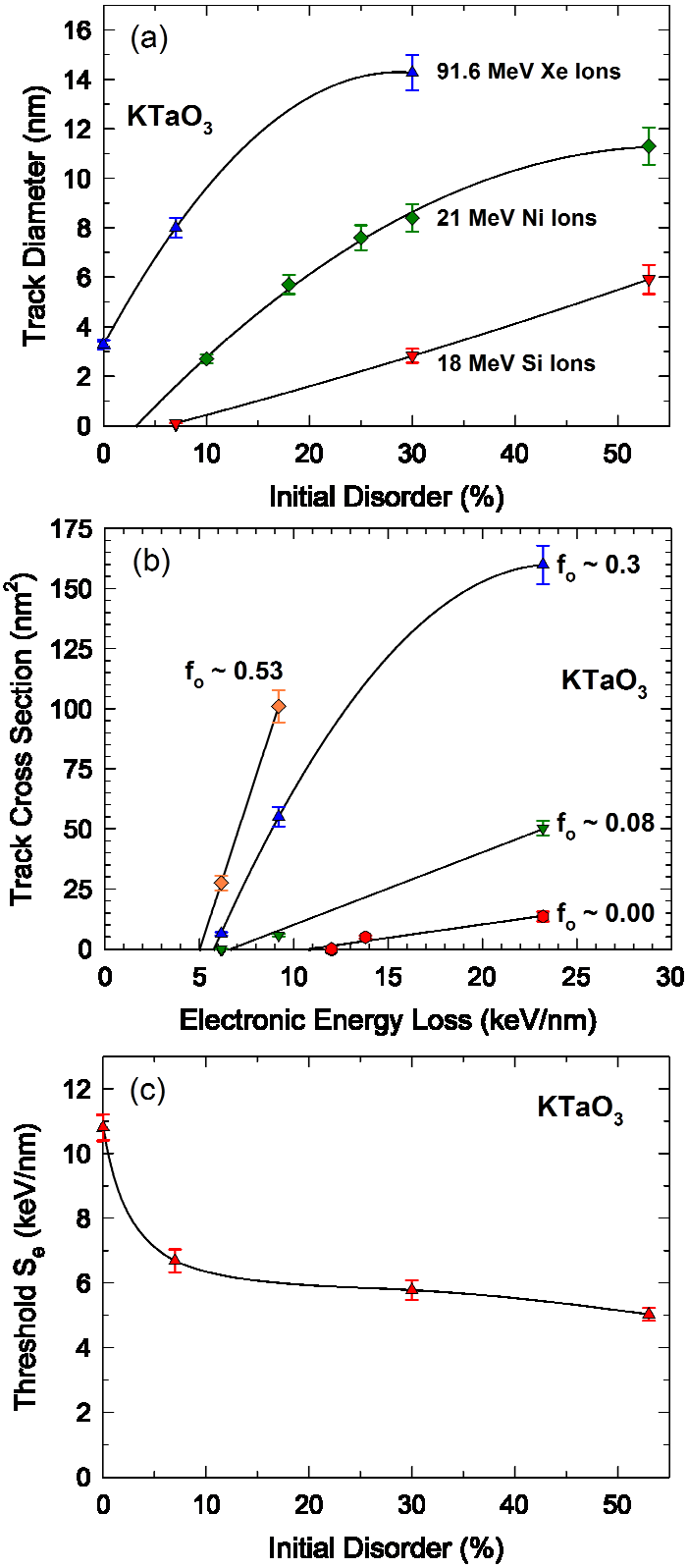

Fig. 6. Track formation in pre-damaged $KTaO_3$ at 300 K: (a) dependence of track diameter on initial disorder; (b) track cross section as a function of electronic energy loss; and (c) dependence of S_e^{th} for track formation on initial disorder. The error bars in determining track diameter is estimated to be ~ 10%, which is mainly attributed to the standard deviation in track cross section from fit of direct impact model [31].

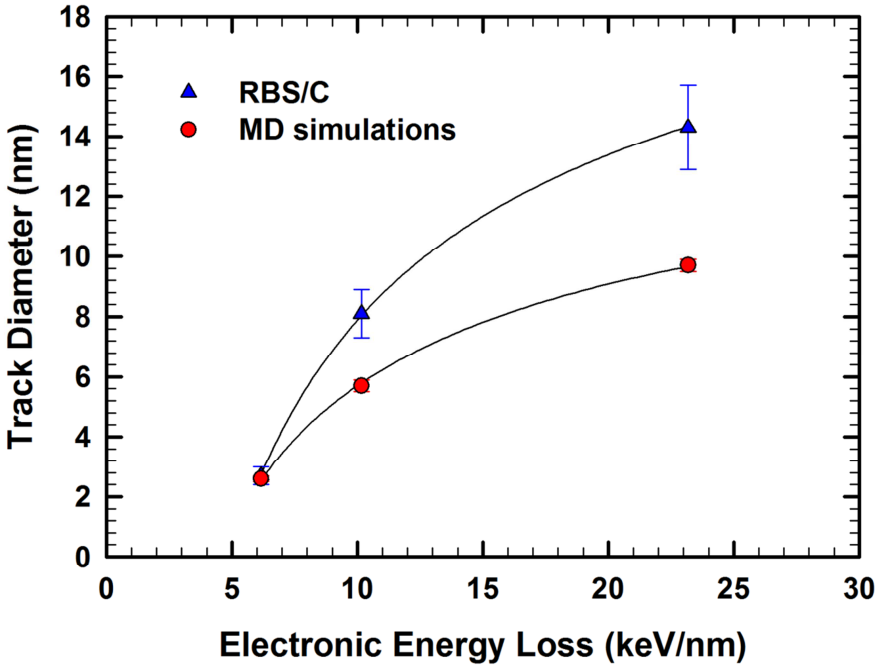

Fig. 7. Comparison of the determined track sizes via RBS/C and MD in pre-damaged $KTaO_3$ with an initial disorder level of $f_0 = 0.33$ and 30 % preexisting FPs, respectively (the error bars are ~10% [31]). The curves in Fig. 7 are just polynomial fits to the data.

Supplementary Material

Near-surface modification of defective KTaO3 by ionizing ion irradiation

G. Velişa[a,b,e*], E. Zarkadoula[b], D. Iancu[a,f], M.D. Mihai[a], C. Grygiel[d], I. Monnet[d], B. Kombaiah[b], Y. Zhang[b,c], and W.J. Weber[c,b**]

[a]Horia Hulubei National Institute for Physics and Nuclear Engineering, Măgurele, IF 077125, Romania
[b]Materials Science and Technology Division, Oak Ridge National Laboratory, Oak Ridge, TN 37831, USA
[c]Department of Materials Science & Engineering, University of Tennessee, Knoxville, TN 37996, USA
[d]Centre de Recherche sur les Ions, les Matériaux et la Photonique, ENSICAEN, UNICAEN, CEA, CNRS, CIMAP, Normandie Université, 14000 Caen, France
[e]Extreme Light Infrastructure–Nuclear Physics (ELI–NP), Măgurele, IF 077125, Romania
[f]University of Bucharest, Faculty of Physics, Măgurele, IF 077125, Romania

RBS/C spectra

The RBS/C spectra for 18 MeV Si irradiated single crystal $KTaO_3$, with an initial damage created by 2 MeV Au ions, are shown in Fig. S1, along with the random equivalent and channeling spectra from the pristine sample. As shown in Fig. S1a, 18 MeV Si ions do not produce significant damage in $KTaO_3$ when a very low initial pre-damage state (relative disorder peak of 0.08) is present. The inset of Fig. S1a presents the RBS/C spectra recorded before and after irradiation with 18 MeV Si ions to a fluence of 8.0×10^{12} ions/cm^2. These spectra do not exhibit any perceptible difference in yield, beyond the uncertainty of the experimental measurements, indicating that 18 MeV Si irradiation did not induce any significant damage in the near surface region (≤1 μm) accessible to RBS/C. Similar results have been previously reported for 21 MeV Ni ions [1]. In contrast, the RBS/C spectra in Fig. S1b clearly exhibit enhanced damage accumulation under 18 MeV Si irradiation when a higher pre-existing damage state (relative disorder peak of 0.3) is present, as evidenced by rapid increase in the Sr and Ti yields with increasing Si ion fluence. The damage accumulation is accelerated with increasing level of pre-existing disorder in $KTaO_3$, as shown in Fig. S1c (relative disorder peak of 0.53).

The high-channel region of the ion channeling spectra (i.e., the Ta sublattice) from the 91.6 MeV Xe irradiated pristine $KTaO_3$ single crystals is shown in Fig. S2a,

together with the random and channeling spectra from a pristine crystal. The spectra recorded in the <100>-axial direction on the Xe-irradiated crystals exhibit, as compared to those for pristine samples, an increase in the backscattering yield with increasing ion fluence due to the accumulation of ionization-induced damage. The ion channeling spectra recorded from Au-irradiated $KTaO_3$ with and without subsequent irradiation with 91.6 MeV Xe ions, are shown in Fig. 2b and c. As shown in Fig. S2b and c, the presence of pre-existing damage states accelerates the increase in the backscattering yield, which suggests that substantially more damage is produced in the defective lattice than in the pristine region. This rapid increase in backscattering yields at low Xe ion fluences indicate direct impact amorphization along the ion path. The irradiation-induced fractional disorder due to 91.6 MeV Xe ions in $KTaO_3$ is quantified by the ratio, *r,* of the relative backscattering yield to the amorphous level: $r = (\chi_d - \chi_p)/(\chi_a - \chi_p)$, where χ_d, χ_p and χ_a are the backscattering yields at 170 nm (channel 1718) in the irradiated region, in the pristine reference sample without ion irradiation and in amorphous $KTaO_3$, respectively. This procedure has been previously used to quantify the high energy ion irradiation-induced disorder in other ABO_3 (e.g., $SrTiO_3$ [R2] and $LiTaO_3$ [R3]) and semiconductors (e.g., InP [4,5], InSb [R4], GaAs [R4], GaP [5], Ge [5], and Si [R4]). The measured damage profiles, shown in Fig. 1 and 2 for the Au ion irradiations, exhibit a nearly Gaussian shape with the damage maximum appearing at a depth of about 170 nm, i.e. very close to the maximum of the SRIM-predicted damage peak (Fig. 1b); this is why the ratio, *r*, is calculated at 170 nm. The RBS/C spectra plotted in Fig. S2a reveal that irradiation of pristine $KTaO_3$ with 91.6 MeV Xe to an ion fluence of 1.0×10^{11} ions/cm^2 leads to a small, but measurable, increase in the value of *r* (from 0.0 % to ~0.21 %). As 91.6 MeV Xe ion fluence increases from 1.0×10^{11} to 1.0×10^{12} ions/cm^2, the value of *r* increases significantly from ~0.21 to 10.4 %. As shown in Fig. S2b, the presence of a low initial level of damage (~0.08) enhances the increase of the ratio *r* (from ~12 to 59 %). This suggests that the average amorphous cross-sections are larger in the pre-damaged regions than in the pristine regions.

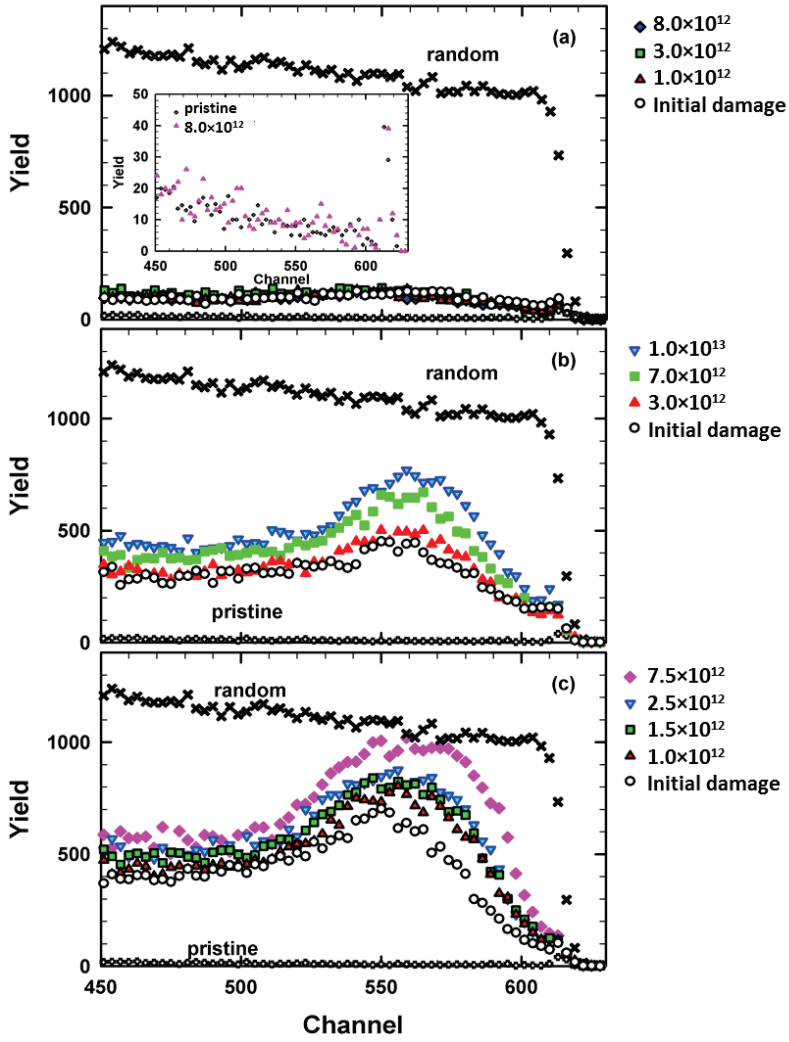

Figure S1: Several RBS/C spectra, after irradiation with 18 MeV Ni for defective $KTaO_3$ with a maximum disorder level of: (a) 0.08, (b) 0.3, and (c) 0.53. The inset shows the RBS/C results for 18 MeV Si irradiations on pristine $KTaO_3$ for an identical ion fluence of 8.0×10^{12} ions/cm^2. Random and channeling spectra from a pristine $KTaO_3$ sample are also included.

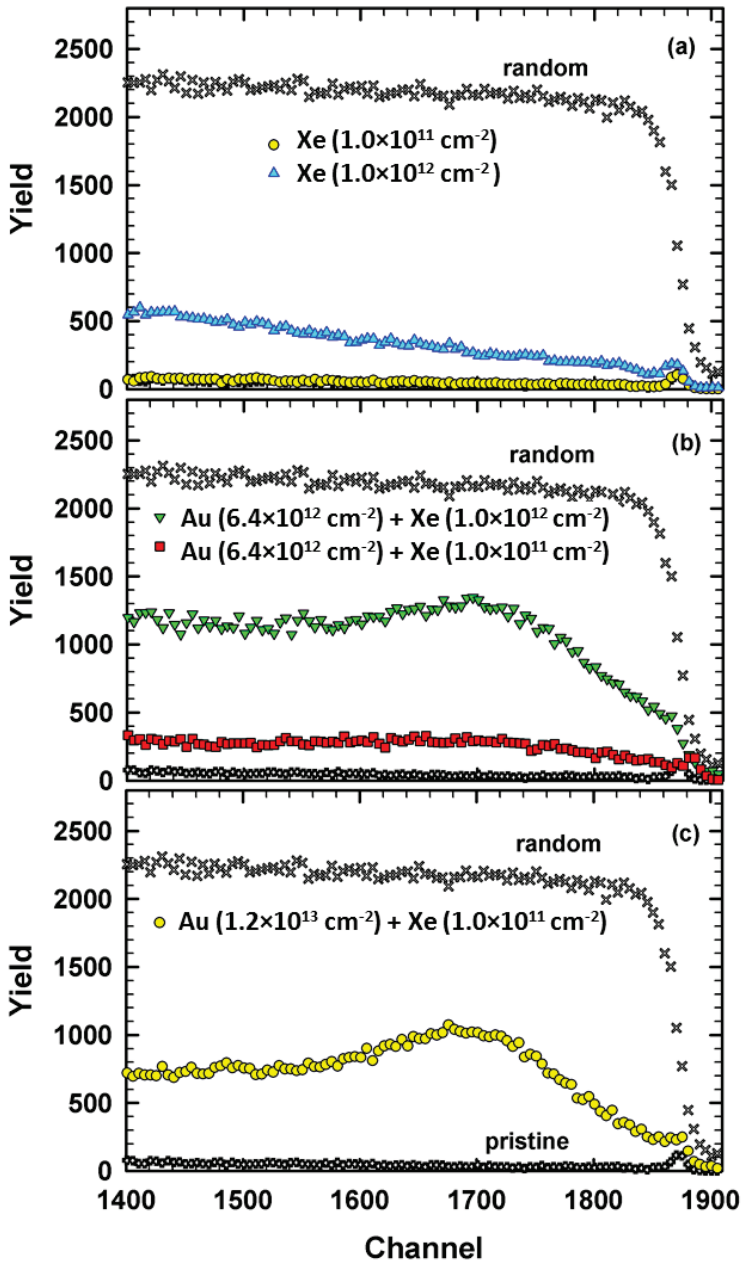

Figure S2: Several RBS/C spectra, after irradiation with 91.6 MeV Xe for: (a) pristine $KTaO_3$ without pre-damage, (b) defective $KTaO_3$ with a maximum disorder level of 0.08, and (c) defective $KTaO_3$ with a maximum disorder level of 0.33. Random and channeling spectra from a pristine $KTaO_3$ sample are also included.

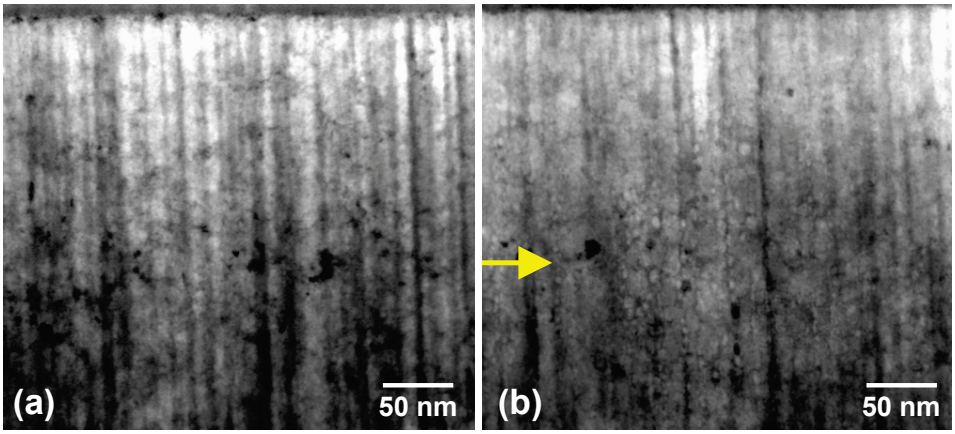

Fig. S3. $KTaO_3$ irradiated with 91.6 MeV ^{129}Xe ions to a fluence of 10^{12} ions/cm^2: (a) pristine sample; (b) sample pre-damage with 2 MeV Au ions to a fluence of 6.4 x 10^{12} ions/cm^2. The yellow arrow indicates the depth of the pre-damaged peak.

TEM results

The irradiated samples were fragile and beam sensitive. The cross-sectional TEM images for pristine and pre-damaged $KTaO_3$ are shown in Fig. S3. The high density of tracks in the pristine irradiated sample is visible in Fig. S3(a) and consistent with the ion fluence. These observations of high track densities in $KTaO_3$ for a high value of S_e (23.18 keV/nm) are consistent with the discontinuous track formation reported by Han et al. [6] in pristine $KTaO_3$ irradiated with 358 MeV Ni ions at lower values of S_e (13.8 keV/nm), which is close to the threshold for track formation. In the pre-damaged sample, there is some evidence for individual ion tracks near the surface, but in the highly pre-damaged region, individual tracks are obscured by the pre-existing damage, as shown in Fig. S3(b).

References

[1] Jin K, Zhang Y and Weber W J 2018 Synergistic effects of nuclear and electronic energy deposition on damage production in $KTaO_3$ *Mater. Res. Lett.* **6** 531–6

[2] Xue H, Zarkadoula E, Sachan R, Zhang Y, Trautmann C and Weber W J 2018 Synergistically-enhanced ion track formation in pre-damaged strontium titanate by energetic heavy ions *Acta Mater.* **150** 351–9

[3] Sellami N, Crespillo M L, Zhang Y and Weber W J 2018 Two-stage synergy of electronic energy loss with defects in $LiTaO_3$ under ion irradiation *Mater. Res. Lett.* **6** 339–44

[4] Kamarou A, Wesch W, Wendler E, Undisz A and Rettenmayr M 2006 Swift heavy ion

irradiation of InP: Thermal spike modeling of track formation *Phys. Rev. B - Condens. Matter Mater. Phys.* **73** 184107

[5] Kamarou A, Wesch W, Wendler E, Undisz A and Rettenmayr M 2008 Radiation damage formation in InP, InSb, GaAs, GaP, Ge, and Si due to fast ions *Phys. Rev. B - Condens. Matter Mater. Phys.* **78** 054111

[6] X. Han, Y. Liu, Q. Huang, M.L. Crespillo, P. Liu, X. Wang, Swift heavy ion tracks in alkali tantalate crystals: a combined experimental and computational study, J. Phys. D. Appl. Phys. 53 (2020) 105304. doi:10.1088/1361-6463/AB5EE6.